First results from the new PVLAS apparatus: A new limit on vacuum magnetic birefringence

F. Della Valle and E. Milotti

INFN, Sezione di Trieste and Dipartimento di Fisica, Università di Trieste,
Via Valerio 2, I-34127 Trieste, Italy

A. Ejlli, G. Messineo, L. Piemontese, and G. Zavattini

INFN, Sezione di Ferrara and Dipartimento di Fisica, Università di Ferrara,
Polo Scientifico, Via Saragat 1C, I-44100 Ferrara, Italy

U. Gastaldi

INFN, Sezione di Ferrara, Polo Scientifico, Via Saragat 1C, I-44100 Ferrara, Italy

R. Pengo and G. Ruoso

INFN, Laboratori Nazionali di Legnaro, Viale dell'Università 2, I-35020 Legnaro, Italy

Several groups are carrying out experiments to observe and measure vacuum magnetic birefringence, predicted by quantum electrodynamics (QED). We have started running the new PVLAS apparatus installed in Ferrara, Italy, and have measured a noise floor value for the unitary field magnetic birefringence of vacuum $\Delta n_u^{(\text{vac})} = (4 \pm 20) \times 10^{-23}$ T^{-2} (the error represents a 1σ deviation). This measurement is compatible with zero and hence represents a new limit on vacuum magnetic birefringence deriving from nonlinear electrodynamics. This result reduces to a factor of 50 the gap to be overcome to measure for the first time the value of $\Delta n_u^{(\text{vac,QED})}$ predicted by QED: $\Delta n_u^{(\text{vac,QED})} = 4 \times 10^{-24}$ T^{-2}. These birefringence measurements also yield improved model-independent bounds on the coupling constant of axion-like particles to two photons, for masses greater than 1 meV, along with a factor-2 improvement of the fractional charge limit on millicharged particles (fermions and scalars), including neutrinos.

I. INTRODUCTION

Nonlinear electrodynamic effects in vacuum have been predicted since the earliest days of quantum electrodynamics (QED), a few years after the discovery of positrons [1–3]. One such effect is vacuum magnetic birefringence [4], closely connected to elastic light-by-light interaction. The effect is extremely small and has never yet been observed directly.

Although today QED is a very well-tested theory, the importance of detecting light-by-light interaction remains. First, QED has always been tested in the presence of charged particles either in the initial state or the final state. No tests exist in systems with only photons. More in general, no interaction has ever been observed directly between gauge bosons present in both the initial and final states. Second, to date, the evidence for zero-point quantum fluctuations relies entirely on the observation of the Casimir effect, which applies to photons only. Here we are dealing with the fluctuations of virtual charged particle-antiparticle pairs (of any nature, including hypothetical millicharged particles) and therefore the structure of fermionic quantum vacuum: to leading order, it would be a direct detection of loop diagrams. Finally, the observation of light-by-light interaction would be an evidence of the breakdown of the

superposition principle and of Maxwell's classical equations. One important consequence of a nonlinearity is that the velocity of light would now depend on the presence or not of other electromagnetic fields.

In a general framework of nonlinear electrodynamics at the lowest order described by a Lorentz invariant parity-conserving Lagrangian correction [5]

$$L_{\text{nl}} = \frac{\xi}{2\mu_0} \left[\eta_1 \left(\frac{E^2}{c^2} - B^2 \right)^2 + 4\eta_2 \left(\frac{\vec{E}}{c} \cdot \vec{B} \right)^2 \right], \quad (1)$$

the induced birefringence due to an external magnetic field perpendicular to the propagation direction of light is

$$\Delta n^{(\text{vac})} = 2\xi(\eta_2 - \eta_1)B^2 = \Delta n_u^{(\text{vac})}B^2. \quad (2)$$

Here $\xi = 1/B_{\text{crit}}^2$ ($B_{\text{crit}} = m^2c^2/e\hbar = 4.4 \times 10^9$ T), and η_1 and η_2 are dimensionless parameters depending on the chosen model. In analogy to what is done for the Cotton-Mouton effect (for a review see Ref. [6]), we have defined the unitary field magnetic birefringence of vacuum $\Delta n_u^{(\text{vac})}$. Moreover, vacuum magnetic birefringence due to axion-like particles (ALP) and millicharged particles also depends

on B^2 [7–11]. These last two hypothetical effects represent new physics beyond the Standard Model and can be searched for in a model-independent way with an apparatus such as Polarizzazione del Vuoto con LASer (PVLAS). In particular, ALPs in the mass range up to 1 meV have long been considered as cold dark matter candidates [12].

In the Euler-Heisenberg electrodynamics $\eta_1^{(QED)} = \frac{4}{7}\eta_2^{(QED)} = \alpha/(45\pi)$, with $\alpha = e^2/(\hbar c 4\pi\epsilon_0)$ being the fine structure constant. In this case,

$$\Delta n_u^{(\text{vac,QED})} = \frac{2}{15\mu_0}\frac{\alpha^2 \bar{\lambda}_e^3}{m_e c^2} = 3.97 \times 10^{-24} \text{ T}^{-2}. \quad (3)$$

The ellipticity ψ induced on a beam of linearly polarized laser light of wavelength λ which traverses a vacuum region of length L, where a magnetic field B orthogonal to the direction of light propagation is present, is given by [13–17]

$$\psi = \frac{N\pi\Delta n_u^{(\text{vac})} \int_0^L B^2 dl}{\lambda} \sin 2\vartheta, \quad (4)$$

where ϑ is the angle between the directions of the polarization vector and of the magnetic field vector and N is the number of times the medium is traversed by the light.

An ellipsometric method to observe vacuum magnetic birefringence was proposed by E. Iacopini and E. Zavattini in 1979 [13]. Experimental attempts started in the 1990s [7,14], and several are ongoing [10,11,15–18]. The Lagrangian (1) also predicts direct light-light elastic scattering. See Refs. [19–24] for experimental attempts. Neither method has reached the capability of detecting this fundamental nonlinear effect regarding light-by-light interaction. Presently published results on $\Delta n_u^{(\text{vac})}$ determined from ellipsometric experiments are reported in Table I.

In this paper, we report on a significant improvement obtained after the commissioning of the new PVLAS experimental setup installed at the INFN section of Ferrara. The principle of the experiment is explained in Refs. [13,16]. The calibration of the apparatus has been done by measuring the Cotton-Mouton effect of O_2 and He gases at low pressures and controlling their consistency with the values present in literature. In this paper, we briefly summarize the main features of the new experimental setup

and focus on the measurements giving a new conservative upper limit on $\Delta n_u^{(\text{vac})}$.

II. EXPERIMENTAL METHOD AND APPARATUS

The upper and lower panels of Fig. 1 show a schematic top view and a photograph of the apparatus.

Linearly polarized laser light from a 2 W Nd:YAG laser is injected into the ellipsometer, which is installed inside a high-vacuum enclosure constructed with nonmagnetic materials and pumped by turbomolecular and nonevaporable getter pumps. The ellipsometer consists of an entrance polarizer **P** and an analyzer **A** set to maximum extinction (nominal extinction ratio $\sigma^2 < 10^{-7}$). Between **P** and **A** are installed the entrance mirror **M1** and the exit mirror **M2** of a 3.303 m long Fabry-Perot cavity **FP** with ultrahigh finesse $\mathcal{F} = 670000$ [26]. The light backreflected by the **FP** is detected by the photodiode **PRF**, and is used by a feedback system which locks the laser frequency to the **FP** with a variant of the Pound-Drever-Hall technique [27]. The resonant light between the two mirrors traverses the bore of two identical permanent 2.5 T dipole magnets in Halbach configuration with $\int B^2 dl = 10.25$ T^2 m and stray field < 1 G at 20 cm along the axis. The magnets can rotate around the **FP** cavity axis up to 10 Hz so that the magnetic field vectors of the two magnets rotate in planes normal to the path of the light stored in the cavity. The motors driving the two magnets are controlled by two phase-locked signal generators. The same signal generators trigger the data
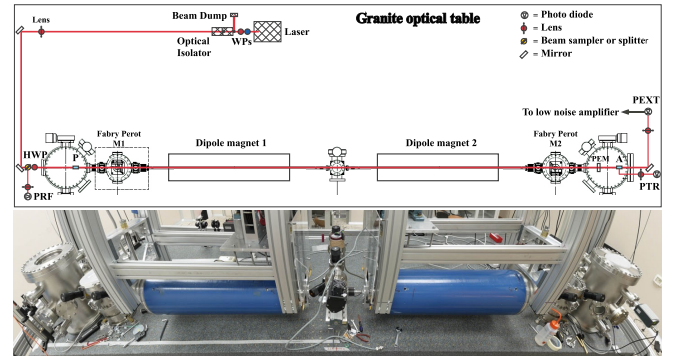

FIG. 1 (color online).   Upper panel: Scheme of the apparatus. The 4.5 ton granite optical table, $4.8 \times 1.5 \times 0.5$ m^3, is shown together with the optical components and the five vacuum chambers. **HWP** = Half wave plate; **P** = Polarizer; **A** = Analyzer; **WPs** = Wave plates; **PEM** = Photoelastic modulator; **PRF** = Reflection photodiode;   **PTR** = Transmission photodiode; **PEXT** = Extinction photodiode. Lower panel: A wide-angle picture of the PVLAS apparatus. The two blue cylinders are the permanent magnets. Each magnet is 96 cm long, has an external diameter of 28 cm, weighs 450 kg, and has a central bore of 20 mm. They are hanging from an aluminium structure mechanically decoupled from the rest of the optical table, which is seismically isolated.

TABLE I.   Presently published results on $\Delta n_u^{(\text{vac})}$ obtained from ellipsometric measurements. Values are in 10^{-23} T^{-2}.

Experiment	Central value	1σ	References
BFRT	22000	2400	[7]
PVLAS-LNL	640	780	[15]
PVLAS-FE test setup	840	400	[16]
BMV	830	270	[25]

acquisition. The magnetic field of the magnets induces a birefringence on the medium in the bores; the **FP** enhances the ellipticity acquired by the light by a factor $N = 2\mathcal{F}/\pi$. Due to the rotation of the magnetic field, the induced ellipticity varies harmonically at twice the rotation frequency of the magnets [see the dependence of ψ from 2ϑ in equation (4)]. Given the parameters of our apparatus ($\lambda = 1064$ nm, $\int B^2 dl = 10.25$ T^2 m), the predicted ellipticity generated by vacuum magnetic birefringence after a single passage of the light through the magnets is $\psi_{\text{single}} = 1.2 \times 10^{-16}$. The **FP** cavity multiplies the single-pass ellipticity ψ_{single} by a factor $N = 4.3 \times 10^5$, resulting in an ellipticity to be measured of $\psi^{(\text{vac,QED})} = 5 \times 10^{-11}$.

A resonant photo elastic modulator (**PEM**) then adds a known small ellipticity ($\eta_0 \approx 10^{-3}$) at a frequency $\Omega_{\text{PEM}} = 50047$ Hz. Under these conditions, the intensity $I_{\text{out}}(t)$ of the light emerging from the analyzer **A** is

$$I_{\text{out}}(t) = I_0[\sigma^2 + |\iota\eta(t) + \iota\psi \sin 2\vartheta(t) + \iota\alpha(t)|^2]$$
$$\simeq I_0[\sigma^2 + \eta(t)^2 + 2\eta(t)\psi \sin 2\vartheta(t) + 2\eta(t)\alpha(t)],$$
$$(5)$$

where I_0 represents the light power reaching the analyzer, $\eta(t)$ is the ellipticity modulation generated by the **PEM**, σ^2 is the extinction ratio of the two polarizers, and $\alpha(t)$ describes the slowly varying spurious ellipticities present in the apparatus. As can be seen, the introduction of the **PEM** linearizes the ellipticity signal, which would otherwise be quadratic. The light emerging from the analyzer is collected by the photodiode **PEXT**.

The most important Fourier components of $I_{\text{out}}(t)$ come from the terms $2\eta(t)\psi \sin 2\vartheta(t)$ and $\eta(t)^2$. The first of these terms results in the beating of the ellipticity induced by the **PEM** (at Ω_{PEM}), and the ellipticity induced by the rotating magnets (at $2\Omega_{\text{Mag}}$). The term $\eta(t)^2$ generates a Fourier component at $2\Omega_{\text{PEM}}$.

During acquisition, the photodiode signal coming from **PEXT** is therefore demodulated at the frequency Ω_{PEM} and at its second harmonic $2\Omega_{\text{PEM}}$. Both these demodulated signals, respectively $I_{\Omega_{\text{PEM}}}(t)$ and $I_{2\Omega_{\text{PEM}}}(t)$, are acquired by a data acquisition system together with the ordinary beam intensity I_0 exiting the analyzer **A**. With the DC component of $I_{2\Omega_{\text{PEM}}}(t)$, indicated as $I_{2\Omega_{\text{PEM}}}(\text{DC})$, and $I_{\Omega_{\text{PEM}}}(t)$, the ellipticity signal $\psi(t)$ can be determined by the equation

$$\psi(t) = \frac{I_{\Omega_{\text{PEM}}}(t)}{\sqrt{8I_0 I_{2\Omega_{\text{PEM}}}(\text{DC})}}.$$
$$(6)$$

With the magnets rotating at Ω_{Mag}, a magnetically induced birefringence will generate a Fourier component of $\psi(t)$ at $2\Omega_{\text{Mag}}$.

Magnetic field sensors and laser locking signals are also acquired to determine the phase of $\psi(t)$ and for diagnostics.

TABLE II. Vacuum equivalent pressures P_{eq} for various gases.

Gas	Δn_u [T^{-2} atm^{-1}]	P_{eq} [mbar]
He	2.1×10^{-16}	2×10^{-5}
Ar	7×10^{-15}	6×10^{-7}
H$_2$O	6.7×10^{-15}	6×10^{-7}
CH$_4$	1.6×10^{-14}	3×10^{-7}
O$_2$	-2.5×10^{-12}	2×10^{-9}
N$_2$	-2.5×10^{-13}	2×10^{-8}

These signals are sampled at 32 times the rotation frequency of the magnets (typically 3 Hz) by a 16-bit multichannel ADC board.

The vacuum system must guarantee that the presence of residual gas species does not mask vacuum magnetic birefringence. Indeed, the Cotton-Mouton effect induces a magnetic birefringence in gases which depends on B^2 exactly like vacuum magnetic birefringence. The magnetic birefringence of gases also depends linearly on pressure. In Table II, the equivalent partial pressures P_{eq} which would mimic a vacuum magnetic birefringence for various gases [6,28–30] are reported. The vacuum system must maintain these species well below their vacuum equivalent pressures. The total pressure is below 10^{-7} mbar, mainly due to H$_2$O.

III. CALIBRATION

Calibration of the apparatus is done using the Cotton-Mouton effect. In this case we used low-pressure oxygen, which gives large signals. More importantly, we have also checked the calibration of the apparatus with low-pressure helium, so as to induce a small ellipticity and demonstrate the sensitivity of the entire system. The lowest pressure of helium used was $P^{(\text{He})} = 32$ μbar. Considering that the unitary birefringence ($B = 1$ T and pressure $= 1$ atm) of helium due to the Cotton-Mouton effect is $\Delta n_u^{(\text{He})} = (2.1 \pm 0.1) \times 10^{-16}$ T^{-2} atm^{-1} [28,29], the birefringence induced at $B = 2.5$ T and $P = 32$ μbar is $\Delta n^{(\text{He})} = 3.9 \times 10^{-20}$. In Fig. 2, the Fourier transform of the measured ellipticity signal $\psi(t)$ is shown. There is a clear peak at $2\Omega_{\text{Mag}}$, corresponding to an ellipticity of $(1.13 \pm 0.13) \times 10^{-7}$, with no spurious peaks present at other harmonics. The integration time was $T = 4$ hours. Given that $\mathcal{F} = 6.7 \times 10^5$, $\lambda = 1064$ nm, and $\int B^2 dl = 10.25$ T^2 m, from the amplitude of the He peak at 32 μbar, the value of Δn_u for helium, $\Delta n_u^{(\text{He,PVLAS})} = (2.7 \pm 0.3) \times 10^{-16}$ T^{-2} atm^{-1}, results in agreement with other published values [6,28,29]. It must be noted that this value is obtained from a single low-pressure point. Two other low-pressure points were also taken. Figure 3 shows a graph of $\Delta n^{(\text{He})}/B^2$ as a function of pressure P.

The calibration process also allows the determination of the physical phase of the Fourier components: the ellipticity induced by a magnetic birefringence is maximum when the
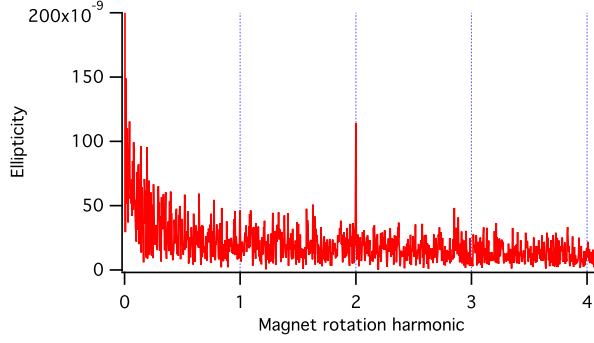
FIG. 2 (color online). Fourier spectrum of the measured ellipticity $\psi(t)$ with 32 μbar pressure of He. The integration time was $T = 4$ hours. The peak at $2\Omega_{Mag}$ corresponds to $\psi = 1.13 \times 10^{-7}$. The vacuum magnetic birefringence predicted by QED is equivalent to a He pressure of $\sim$20 nbar.
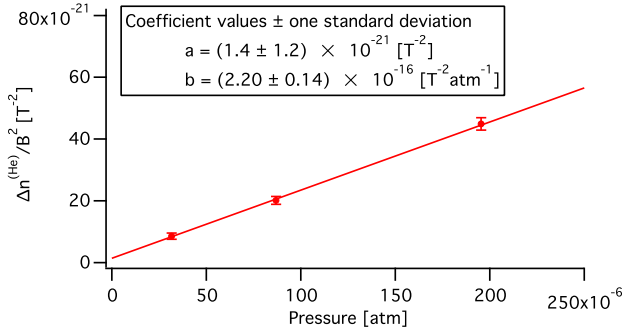

FIG. 3 (color online). Measured $\Delta n^{(He)}/B^2$ as a function of pressure P. The error bars correspond to a 1σ statistical error. The data are fitted with a linear function $a + bP$.

magnetic field is at $\vartheta = \pm45°$ with respect to the polarization direction. Since a magnetic birefringence can be either positive or negative, the physical phase is determined mod 180°. A magnetically induced birefringence must have a phase consistent with the calibration phase. The ellipticity amplitudes determined from the Fourier transforms of the data obtained in vacuum are therefore projected along the physical axis and along the nonphysical orthogonal axis.

IV. RESULTS

The data presented in this paper have been collected by rotating the two magnets at frequencies ranging from 2.4 to 3 Hz for a total of 210 hours. Of these, 40 hours have been acquired with the magnets rotating at slightly different frequencies so as to check that neither of the two was generating spurious signals.

The data analysis procedure is as follows:
(1) For each run, lasting typically one day, the acquired signals are subdivided into blocks of 8192 points (256 magnet revolutions), and a Fourier transform of the ellipticity signal $\psi(t)$, calculated using equation (6), is taken for each block.

(2) For each block, the average noise in the ellipticity spectrum around $2\Omega_{Mag}$ is taken. The ellipticity amplitude noise follows the Rayleigh distribution $P(\rho) = (\rho/\sigma^2)e^{-\frac{\rho^2}{2\sigma^2}}$, in which the parameter σ represents the standard deviation of two identical independent Gaussian distributions for two variables x and y, and $\rho = \sqrt{x^2 + y^2}$. In our case, x and y represent the projections of the ellipticity value at $2\Omega_{Mag}$ along the physical and the nonphysical axes. The average of $P(\rho)$ is related to σ by $\langle P \rangle = \sigma\sqrt{\pi/2}$. For each data block, σ is determined. This value is used in the next step as the weight for the ellipticity value at $2\Omega_{Mag}$.
(3) For each run, a weighted vector average of the Fourier components of the ellipticities at $2\Omega_{Mag}$, determined in step 2, is taken.
(4) Using the values for $\mathcal{F}$, $\int B^2 dl$, and λ for each run, $\Delta n/B^2$ and σ/B^2 are determined. $\Delta n/B^2$ is then projected onto the physical and nonphysical axes. These values are plotted in Fig. 4.

The weighted vector average of all the runs results in a value for the unitary birefringence of vacuum, with a 1σ error, of

$$\Delta n_u^{(vac)} \pm \sigma_{\Delta n_u^{(vac)}} = (4 \pm 20) \times 10^{-23} \text{ T}^{-2} \qquad (7)$$

for the physical component (same phase and sign as for the helium Cotton-Mouton birefringence). For the nonphysical component, one finds $\Delta n_u^{(\text{non physical})} \pm \sigma_{\Delta n_u^{(vac)}} = (5 \pm 20) \times 10^{-23}$ T^{-2}. This new limit is about a factor
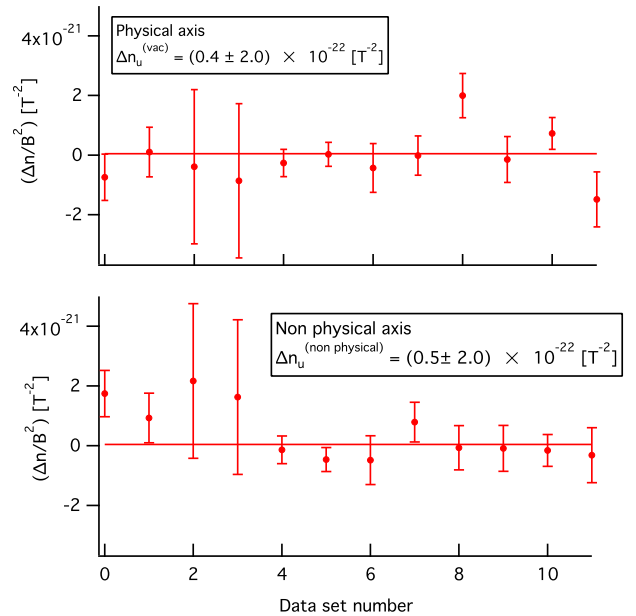

FIG. 4 (color online). Projections of $\Delta n/B^2$ along the physical and the nonphysical axes for all the data sets. The horizontal red line represents the weighed average for all the runs.

of 50 from the predicted QED value of equation (3), $\Delta n_u^{(\text{vac,QED})} = 3.97 \times 10^{-24}$ T^{-2}.

V. DISCUSSION AND CONCLUSIONS

A. QED

We have reported here on a significant improvement in the measurement of the magnetic birefringence of vacuum. In the Euler-Heisenberg framework, we are now only a factor of 50 away from the theoretical parameter, $\Delta n_u^{(\text{vac,QED})} = 3.97 \times 10^{-24}$ T^{-2}, describing this effect. Our new limit is

$$\Delta n_u^{(\text{vac})} \pm \sigma_{\Delta n_u^{(\text{vac})}} = (4 \pm 20) \times 10^{-23} \text{ T}^{-2}. \quad (8)$$

In Fig. 5, we compare previously published results with our new value and with the predicted QED effect.

In the Euler-Heisenberg framework where $\eta_1^{(\text{QED})} = \frac{4}{7}\eta_2^{(\text{QED})} = \alpha/(45\pi)$, the elastic photon-photon total cross section for nonpolarized light depends directly on $\Delta n_u^{(\text{vac,QED})}$. In the limit of low-energy photons, $E_\gamma \ll m_e c^2$ [31–33],

$$\sigma_{\gamma\gamma}^{(\text{QED})}(E_\gamma) = \frac{973\mu_0^2}{180\pi} \frac{E_\gamma^6}{\hbar^4 c^4} (\Delta n_u^{(\text{vac,QED})})^2. \quad (9)$$

From the experimental bound on $\Delta n_u^{(\text{vac})}$, one can therefore place an upper bound on $\sigma_{\gamma\gamma}^{(\text{QED})}$:

$$\sigma_{\gamma\gamma}^{(\text{QED})} < 4.6 \times 10^{-66} \text{ m}^2 @ 1064 \text{ nm} \quad (10)$$

The QED prediction for this number is instead $\sigma_{\gamma\gamma}^{(\text{QED})} = 1.84 \times 10^{-69}$ m^2.

Although the sensitivity of our apparatus is far from its theoretical shot noise limit, integration in the absence of spurious peaks at the frequency of interest has allowed this
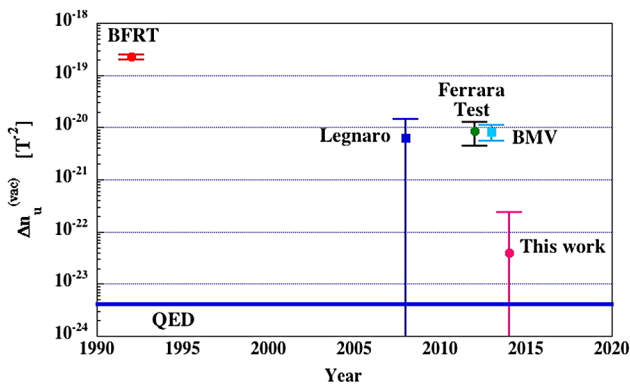

FIG. 5 (color online). Comparison of published results for $\Delta n_u^{(\text{vac})}$ of ellipsometric experiments (BFRT = [7], Legnaro = [15], Ferrara test = [16], BMV = [25]). The error bars correspond to a 1σ C.L.

significant improvement. The origin of the excess noise is still unknown but is clearly due to the presence of the Fabry-Perot cavity; without the cavity, shot noise is achieved. We suspect that the origin of this noise is due to variations in the intrinsic birefringence of the reflective coating due to thermal effects. Nonetheless, at present the ellipsometric technique is the most sensitive one for approaching low-energy nonlinear electrodynamics effects. Efforts will now go into the improvement of the sensitivity.

B. Axion-like particles

Compared to model-dependent constraints deriving from astrophysics [34], limits from laboratory experiments cannot compete. Nevertheless, they can set new model-independent limits on the coupling constant of axion-like particles (ALP) to two photons. In the results presented here, only the runs with both magnets rotating at the same frequency were used, so that the total field length could be taken as the sum of the two magnet lengths.

The magnetic birefringence induced by low mass axion-like particles can be expressed as [7]

$$\Delta n^{(\text{vac,ALP})} = \frac{g_a^2 B^2}{2m_{a,s}^2} \left(1 - \frac{\sin 2x}{2x}\right), \quad (11)$$

where g_a is the ALP-2 photon coupling constant, m_a its mass, $x = \frac{Lm_a^2}{4\omega}$, ω is the photon energy, and L is the magnetic field length. The above expression is in natural Heavyside-Lorentz units, whereby 1 T$= \sqrt{\frac{\hbar^3 c^3}{e^4 \mu_0}} = 195$ eV^2 and 1 m $= \frac{e}{\hbar c} = 5.06 \times 10^6$ eV^{-1}.

In the approximation for which $x \ll 1$ (small masses), this expression becomes

$$\Delta n^{(\text{vac,ALP})} = \frac{g_a^2 B^2 m_a^2 L^2}{48\omega^2}, \quad (12)$$

whereas for $x \gg 1$,

$$\Delta n^{(\text{vac,ALP})} = \frac{g_a^2 B^2}{2m_a^2}. \quad (13)$$

From our limit on $\Delta n_u^{(\text{vac})}$ given in equation (7), one can plot a new model-independent exclusion plot for ALPs. The plot is shown in Fig. 6. Above 10^{-3} eV, there is an improvement on the upper limit of g_a with respect to previously published model-independent limits.

C. Millicharged particles

Slightly better exclusion plots can also be derived from $\Delta n_u^{(\text{vac})}$ for fermion and scalar millicharged particles. The vacuum magnetic birefringence due to the existence of such hypothetical millicharged particles can be calculated following Ref. [35–37]. By defining the ratio of the charge q
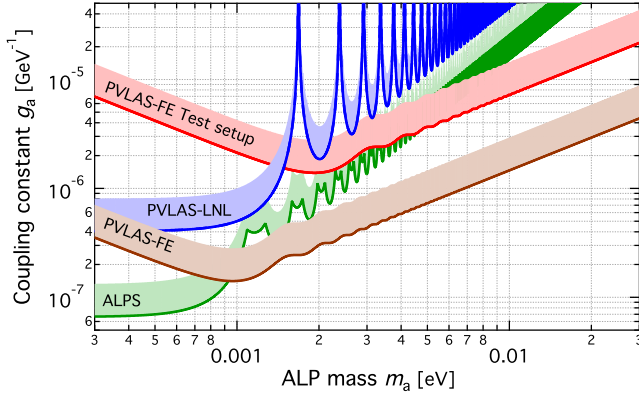
FIG. 6 (color online). Updated 95% C.L. exclusion plot for axion-like particles. In green, limits from the ALPS Collaboration [40] are shown; in blue, limits from dichroism measurements performed by PVLAS at LNL [8]; in red, limits from the ellipticity measurements performed with the test setup in Ferrara [16]. The results described in this paper lead to a new bound, shown in brown. Preliminary results from the OSQAR Collaboration can be found in Ref. [41]. They are very similar to the results from ALPS.

of such particles to the charge of the electron $\epsilon = q/e$ and χ as

$$\chi \equiv \frac{3}{2} \frac{\hbar\omega}{m_e c^2} \frac{\epsilon e B \hbar}{m_e^2 c^2}, \tag{14}$$

it can be shown that

$$\Delta n^{(\text{vac: fermion})}$$

$$= \begin{cases} \Delta n_u^{(\text{MCP})} B^2 & (\chi \ll 1) \\ -\frac{135}{14} \frac{\pi^{1/2} 2^{1/3} (\Gamma(\frac{2}{3}))^2}{\Gamma(\frac{1}{6})} \chi^{-4/3} \Delta n_u^{(\text{MCP})} B^2 & (\chi \gg 1), \end{cases} \tag{15}$$

$$\Delta n^{(\text{vac: scalar})}$$

$$= \begin{cases} -\frac{1}{2} \Delta n_u^{(\text{MCP})} B^2 & (\chi \ll 1) \\ \frac{135}{28} \frac{\pi^{1/2} 2^{1/3} (\Gamma(\frac{2}{3}))^2}{\Gamma(\frac{1}{6})} \chi^{-4/3} \Delta n_u^{(\text{MCP})} B^2 & (\chi \gg 1), \end{cases} \tag{16}$$
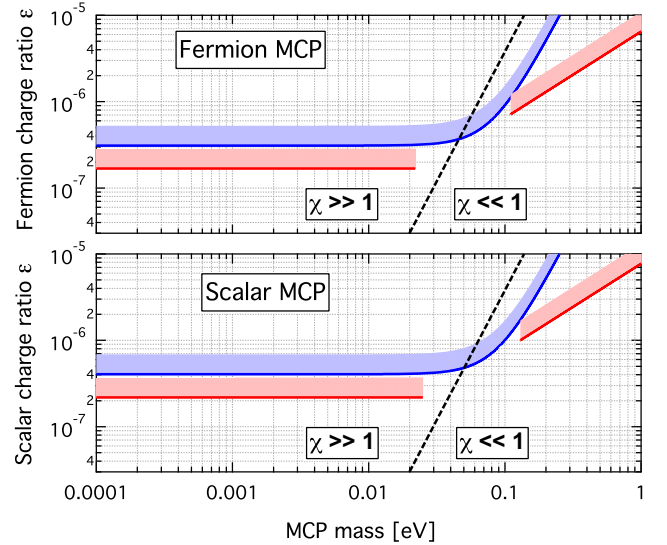

FIG. 7 (color online). Updated 95% C.L. exclusion plot for scalar and fermion millicharged particles. In blue is the previous limit taken from Ref. [38] and in red are our new limits. The two branches of each of the red ellipticity curves are not connected in the mass range around $\chi \simeq 1$ (dotted black line), where the birefringence changes sign.

where, in analogy to QED, $\Delta n_u^{(\text{MCP})}$ is

$$\Delta n_u^{(\text{MCP})} = \frac{2}{15\mu_0} \frac{\epsilon^4 \alpha^2 \lambdabar_e^3}{m_e c^2}. \tag{17}$$

In Fig. 7, we show our new limit on ϵ as a function of particle mass compared to a previous limit obtained from magnetically induced dichroism measurements [38]. In the case of fermions, this includes neutrinos for which $\epsilon \lesssim 10^{-7}$ for masses below 20 meV. For previous limits, see Ref. [39].

ACKNOWLEDGMENTS

We greatly thank Luca Landi from the University of Ferrara for his invaluable technical help during the construction of the apparatus.

[1] H. Euler and B. Kochel, Naturwissenschaften **23**, 246 (1935); W. Heisenberg and H. Euler, Z. Phys. **98**, 714 (1936); V. S. Weisskopf and K. Dan, Vidensk. Selsk. Math. Fys. Medd. **14**, 6 (1936); J. Schwinger, Phys. Rev. **82**, 664 (1951).

[2] P. A. M. Dirac, Proc. R. Soc. A **117**, 610 (1928); **126**, 360 (1930).

[3] C. D. Anderson, Phys. Rev. **43**, 491 (1933).

[4] R. Baier and P. Breitenlohner, Acta Phys. Austriaca **25**, 212 (1967); Nuovo Cimento **47**, 261 (1967); S. L. Adler, Ann. Phys. (N.Y.) **67**, 599 (1971); Z. Bialynicka-Birula and I. Bialynicki-Birula, Phys. Rev. D **2**, 2341 (1970).

[5] V. I. Denisov, I. V. Krivchenkov, and N. V. Kravtsov, Phys. Rev. D **69**, 066008 (2004).

[6] C. Rizzo, A. Rizzo, and D. M. Bishop, Int. Rev. Phys. Chem. **16**, 81 (1997).

[7] R. Cameron, G. Cantatore, A. C. Melissinos, G. Ruoso, Y. Semertzidis, F. Nezrick, C. Rizzo, and E. Zavattini, Phys. Rev. D **47**, 3707 (1993).

[8] E. Zavattini *et al.*, Phys. Rev. D **77**, 032006 (2008).

[9] W.-T. Ni, Chin. J. Phys. **34**, 962 (1996).

[10] H.-H. Mei, W.-T. Ni, S.-J. Chen, and S.-S. Pan, Mod. Phys. Lett. A, **25**, 983 (2010).

[11] P. Pugnat *et al.*, Cesk. Cas. Fyz. **56**, C193 (2006).

[12] P. Arias, D. Cadamuro, M. Goodsell, J. Jaeckel, J. Redondo, and A. Ringwald, J. Cosmol. Astropart. Phys. 06 (2012) 013.

[13] E. Iacopini and E. Zavattini, Phys. Lett. **85B**, 151 (1979).

[14] D. Bakalov *et al.*, Hyperfine Interact. **114**, 103 (1998).

[15] M. Bregant *et al.*, Phys. Rev. D **78**, 032006 (2008).

[16] F. Della Valle, U. Gastaldi, G. Messineo, E. Milotti, R. Pengo, L. Piemontese, G. Ruoso, and G. Zavattini, New J. Phys. **15**, 053026 (2013).

[17] F. Della Valle, G. Di Domenico, U. Gastaldi, E. Milotti, G. Messineo, R. Pengo, L. Piemontese, G. Ruoso, and G. Zavattini, Nucl. Instrum. Methods Phys. Res., Sect. A **718**, 495 (2013).

[18] R. Battesti *et al.*, Eur. Phys. J. D **46**, 323 (2008).

[19] D. Bernard, F. Moulin, F. Amiranoff, A. Braun, J. P. Chambaret, G. Darpentigny, G. Grillon, S. Ranc, and F. Perrone, Eur. Phys. J. D **10**, 141 (2000).

[20] F. Moulin, D. Bernard, and F. Amiranoff, Z. Phys. C **72**, 607 (1996).

[21] E. Lundström, G. Brodin, J. Lundin, M. Marklund, R. Bingham, J. Collier, J. Mendonça, and P. Norreys, Phys. Rev. Lett. **96**, 083602 (2006).

[22] D. Tommasini, A. Ferrando, H. Michinel, and M. Seco, Phys. Rev. A **77**, 042101 (2008).

[23] A. N. Luiten and J. C. Petersen, Phys. Rev. A **70**, 033801 (2004); Phys. Lett. A **330**, 429 (2004).

[24] E. Milotti *et al.*, Int. J. Quantum. Inform. **10**, 1241002 (2012).

[25] A. Cadène, P. Berceau, M. Fouché, R. Battesti, and C. Rizzo, Eur. Phys. J. D **68**, 16 (2014).

[26] F. Della Valle, E. Milotti, A. Ejlli, U. Gastaldi, G. Messineo, L. Piemontese, G. Zavattini, R. Pengo, and G. Ruoso, Opt. Express **22**, 11570 (2014).

[27] G. Cantatore, F. Della Valle, E. Milotti, P. Pace, E. Zavattini, E. Polacco, F. Perrone, C. Rizzo, G. Zavattini, and G. Ruoso, Rev. Sci. Instrum. **66**, 2785 (1995).

[28] M. Bregant *et al.*, Chem. Phys. Lett. **471**, 322 (2009).

[29] A. Cadène, D. Sordes, P. Berceau, M. Fouché, R. Battesti, and C. Rizzo, Phys. Rev. A **88**, 043815 (2013).

[30] F. Della Valle, A. Ejlli, U. Gastaldi, G. Messineo, E. Milotti, R. Pengo, L. Piemontese, G. Ruoso, and G. Zavattini, Chem. Phys. Lett. **592**, 288 (2014).

[31] B. De Tollis, Nuovo Cimento **35**, 1182 (1965); **32**, 757 (1964).

[32] R. Karplus and M. Neuman, Phys. Rev. **83**, 776 (1951).

[33] D. A. Dicus, C. Kao, and W. W. Repko, Phys. Rev. D **57**, 2443 (1998).

[34] J. Jaeckel and A. Ringwald, Annu. Rev. Nucl. Part. Sci. **60**, 405 (2010).

[35] W.-y. Tsai and T. Erber, Phys. Rev. D **12**, 1132 (1975).

[36] J. K. Daugherty and A. K. Harding, Astrophys. J. **273**, 761 (1983).

[37] M. Ahlers, H. Gies, J. Jaeckel, and A. Ringwald, Phys. Rev. D **75**, 035011 (2007).

[38] M. Ahlers, H. Gies, J. Jaeckel, J. Redondo, and A. Ringwald, Phys. Rev. D **77**, 095001 (2008).

[39] K. Nakamura *et al.* (Particle Data Group), J. Phys. G **37**, 075021 (2010).

[40] K. Ehret *et al.* Phys. Lett. B **689**, 149 (2010).

[41] OSQAR Annual Report No. CERN-SPSC-2013-030/SPSC-SR-125, 2013.